JOURNAL OF PROPULSION AND POWER
Vol. 20, No. 1, January–February 2004

Experimental Study on Linear Compressor Cascade with Three-Dimensional Blade Oscillation

H. Yang* and L. He†
University of Durham, Durham, England, DH1 3LE, United Kingdom

An experiment is carried out to enhance the understanding of three-dimensional blade aeroelastic mechanisms and to produce test data for validation of numerical methods. A compressor cascade test rig developed consists of seven prismatic controlled diffusion blades with the middle blade being oscillated in a three-dimensional bending/flapping mode. Steady and unsteady pressure measurements are performed at six spanwise sections for three reduced frequencies and two tip-clearance gaps. Off-board pressure transducers are utilized with a transfer-function method correcting tubing errors. The tuned cascade results are constructed by using the influence coefficient method. The results illustrate fully three-dimensional unsteady behaviour. The blades are aeroelastically destabilized as the tip gap is increased, and the destabilizing effect of the tip-clearance influences most of the span. The total aerodynamic damping at the least stable interblade phase angle is reduced by 27% when the tip gap is increased from nearly 0 to 2% span.

Nomenclature

Am_ℓ = local bending amplitude, nondimensionalized with chord
Am_{tip} = bending amplitude at blade tip, nondimensionalized with chord
Ap_1 = amplitude of the first harmonic pressure, Pa
C = blade chord length
Cax = blade axial chord length
Cp = blade surface pressure coefficient, $Cp = (p - p_2)/(p_{01} - p_2)$
$|Cp_1|$ = amplitude of the first harmonic pressure coefficient, $|Cp_1| = Ap_1/(P_{01} - P_2)/Am_{\text{tip}}$
$|Cp_1(n)|$ = amplitude of the first harmonic pressure coefficient induced on blade n
D = blade bending displacement (normal to chord, positive from P.S. to S.S.)
ds = chordwise length of surface element
f = frequency, Hz
h = blade span, m
k = reduced frequency, $k = \omega C/V_{\text{ref}}$
P_{01} = inlet total pressure at midspan
P_2 = exit static pressure
V_{ref} = reference isentropic exit velocity, ms^{-1}, $V_{\text{ref}} = \sqrt{[2(P_{01} - P_2)/\rho]}$
x = axial chordwise location, m
z = spanwise coordinate, m
β_1 = inlet flow angle, deg
ξ = overall aerodynamic damping coefficient,

$$\xi = \frac{1}{h}\int_h \xi_c \, \mathrm{d}z$$

ξ_c = local aerodynamic damping coefficient,

$$\xi_c = \int_c \frac{-\pi \, Am_\ell |Cp_1| \sin\phi_1}{C \, Am_{\text{tip}}} \, ds$$

σ = interblade phase angle (IBPA), deg
ϕ_1 = phase angle of the first harmonic pressure relative to blade vibration, deg

Subscripts

0 = stagnation flow parameter
1 = inlet parameter; first harmonic
2 = exit parameter; second harmonic

Received 18 March 2003; revision received 25 August 2003; accepted for publication 25 August 2003.

*Ph.D. candidate, School of Engineering.
†Professor, Thermo-Fluid Dynamics, School of Engineering.

I. Introduction

AEROELASTIC problems are a major concern in development of turbomachines. Blade flutter as a common type of such problems typically affects fans, frontal stages of compressors, and rear stages of low-pressure turbines with relatively long blades. Physical understanding and predictive capability of blade flutter remain challenging and have been a major focus of research because the corresponding aeroelastic mechanisms are complex and many variables are involved.

One of notable early experimental studies on main flutter parameters (reduced frequency, incidence, and interblade phase angle) for compressor cascades is the work by Carta and St. Hilarie.[1,2] In the past two decades or so, unsteady flows around various compressor and turbine cascades, oscillating in two-dimensional plunging (bending) and torsion modes, have been tested at subsonic, transonic, and supersonic speeds, typified in the standard configurations compiled by Bölcs and Fransson.[3] The influence of separation bubble on blade aeroelastic stability is experimentally identified for turbine blades by He[4] and for compressors by Buffum et al.[5]

All of the published experimental researches with detailed measurement are, however, limited to two-dimensional sections with data typically taken at midspan of cascades. Although turbomachinery flows are three-dimensional in general, there has also been considerable recent effort in developing fully three-dimensional blading to increase aerothermal performance. Hence, blade aeroelastic and aeromechanical design and analysis will need to be based on fully three-dimensional methodologies, even though they have been conventionally largely two-dimensional or quasi-three-dimensional (as in the strip theory in which each spanwise section is calculated separately). In this context it is particularly worthwhile noting that there have been no published three-dimensional cascade data, which can be directly used to validate three-dimensional blade aeromechanical methods currently under active development.

It is recognized that the experimental testing of oscillating blades in realistic high-speed transonic flow conditions is a very challenging task. In particular, the problem in high-speed flows is compounded by the coexistence of the self-excited unsteadiness of large magnitudes, as indicated by Lepicovsky et al.[6] On the other hand,

there is a large body of evidence demonstrating clearly that low-speed tests can be used to provide high quality data for method validations and to enhance the understanding of important three-dimensional and/or unsteady flow physics, although transonic-flow effects will have to be missed.

Given the need for the three-dimensional experimental data, the authors took the approach of low-speed testing for its simplicity and high data quality, as well as the experience gathered previously in unsteady pressure measurements on two low-speed test rigs.[4,7–9] An experimental study on three-dimensional unsteady flow for a single turbine blade oscillating in three-dimensional bending vibration is documented by Bell.[7] Further experimental work on the same oscillating turbine blade with massive part-span flow separation is conducted by Queune and He[9] to study the steam turbine blade aeroelasticity under low flow off-design conditions. These two pieces of three-dimensional experimental work have formed a sound foundation for the present work, although both are limited to a single turbine blade configuration without the important blade-to-blade interference. In the present experiment this issue is addressed by using the Influence Coefficient Method,[10] resulting in unsteady flow data for a tuned cascade (i.e., all blades are oscillating in the same frequency, the same amplitude, and a constant interblade phase angle).

In the context of three-dimensional flows through blade rows in axial compressors, there are many reported researches on the effects of tip clearance on aerothermal performance and flow stability, for example, Hoying et al.,[11] Kang and Hirsch,[12] and Pandya and Lakshminarayana.[13] The tip-leakage flow is now recognized as an important source of loss and believed to be closely related to the onset of rotating stall in compressors. An investigation on the tip-clearance effect on the aerodynamic damping is performed on a linear cascade of flat plates in a two-dimensional bending oscillation by Watanabe and Kaji.[14] However, the influence of tip clearance on the aeroelastic behavior of realistic compressor blades in a three-dimensional oscillation mode is still unknown. To gain insights into the effect on compressor aeroelastic characteristics and to identify the corresponding unsteady computational-fluid-dynamics modeling requirement, unsteady pressure responses under different tip gaps are also investigated in this experiment.

II. Experimental Facility And Methods

A. Low-Speed Linear Cascade Rig

A new low-speed test facility is purposely built for the current experimental work. It is an open flow facility with a rectangular test cross section of 250×800 mm. The flow discharge from a centrifugal fan (powered by an 11-kW motor) is diffused into a large settling chamber, then is driven through a shaped contraction (contraction ratio of 7.5:1) into the test section, and then exhausted to the ambient. Table 1 shows the operational conditions established during the design of the test facility.

A linear cascade is located in the exhaust part of the tunnel, which consists of seven blade airfoils, wooden frames, perspex sidewalls, profiled upper wall and lower wall, as shown in Fig. 1. The required inlet flow angle is adjusted by rotating the cascade around a horizontal axis at the top end. The tunnel side-wall boundary layers are removed by side bleeding one chord length upstream of the blade leading edge. The bleeding is adjusted to improve the blade–blade periodicity. The reference oscillating blade (blade 0, as shown in Fig. 2) is hinged at blade hub on the perspex side wall and is driven at the blade tip to produce a sinusoidal movement by a crank bar mechanism. Thus the bending amplitude varies linearly along the blade span. To reduce the leakage from the tip end wall caused by the bar link between the moving blade and the driving mechanism and from the hub end wall caused by the outside root hinge, foam tapes, card and dense sponge are used to block the end-wall slot, while ensuring an unrestricted bending motion of the blade. Table 2 shows the main parameters of the cascade rig. Because the blade-root hinge is positioned outside the test section, there is a very small displacement at the hub section.

The blade profile is the same as the controlled-diffusion blading described by Elazar and Shreeve,[15] which has been extensively studied for its steady flow performance in modern compressor blading designs. This particular blading profile is chosen in order to easily compare baseline steady flow results with those in the open literature (e.g., Sanger and Shreeve[16] and Sasaki and Breugelmans[17]).

Table 1 Summary of operational conditions

Experimental conditions	Value
Inlet flow angle, β_1	37.5 deg
Reynolds number Re (based on blade chord and exit velocity)	1.95×10^5
Typical exit isentropic velocity V_{ref}	19.5 m/s
Reduced frequency range k	0.2, 0.4, 0.6
Nominal frequencies f, Hz at the atmospheric condition	4.14, 8.28, 12.4

Table 2 Airfoil and linear cascade data

Item	Description
Airfoil	
Type	Controlled diffusion airfoil
Chord length, C	0.15 m
Aspect ratio, h/C	1.27
Solidity, C/S	1.67
Maximum thickness	0.07C
Leading-edge radius	0.00132 m
Trailing-edge radius	0.00186 m
Linear cascade	
Number of airfoils	7
Pitch length, S	0.09 m
Blade span, h	0.19 m
Stagger angle, γ	14.2 deg
Bending direction	Normal to the absolute chord (positive P. S. → S. S.)
Bending amplitude at tip, Am_{tip}	0.06C
Bending amplitude at hub	0.005C

Fig. 1 Low-speed linear compressor cascade.

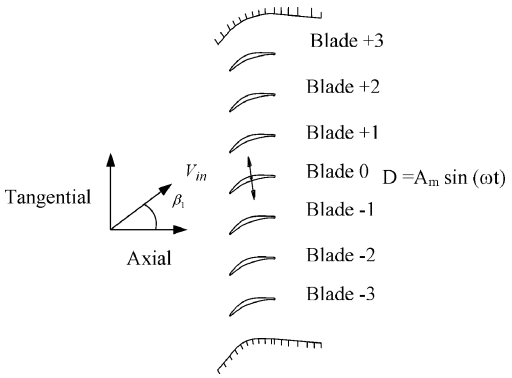

Fig. 2 Linear cascade configuration.

B. Instrumentation and Data Processing

The middle reference blade and one stationary blade are instrumented at six spanwise sections (20, 50, 70, 90, 95, and 98% span). At each spanwise section there are 14 tappings on the suction surface and 10 tappings on the pressure surface. These tappings are used for both steady and unsteady pressure measurements. The instrumented stationary blade can be interchanged with other stationary blades in order to measure unsteady pressure distributions on all blades in the cascade.

The low flow velocity means that a reasonably high reduced frequency can be achieved with a low blade vibration frequency, which makes it convenient to use externally mounted pressure transducers to measure unsteady pressures. This technique avoids the use of expensive miniature flush-mounted pressure transducers and enables detailed measurements over three-dimensional blade surfaces to be conducted very effectively. In the present experiment five Sensym 142C01D pressure transducers are off-board mounted and used for unsteady pressure measurements (30 measurements for each blade with 144 tappings). Unsteady signals from the transducers are discretized and acquired on a PC by an Amplicon PC30G data-logging card. The data-logging process is triggered by an optical Schmitt sensor at a fixed phase of the blade vibration to keep unsteady signals recorded synchronously over all blades. The data-acquisition system is similar to the set-up of Bell and He.[8]

To filter out random noise and disturbances from turbulent fluctuations, pressure signals are ensemble-averaged over 50 periods using Eq. (1).

$$p(n,t) = \frac{1}{N_{\text{enb}}} \sum_{N=1}^{N_{\text{enb}}} p(n, t+NT), \qquad (n = 1, 2, \ldots, n_p) \quad (1)$$

To demonstrate that this number of ensemble averages is sufficient, Fig. 3 shows representative samples of ensemble-averaged unsteady signals recorded at the 14 tappings on the suction surface of the oscillating blade. The traces are vertically shifted for clarity, so that the vertical scale should be taken only in a relative sense. The nonsinusoidal variation shown in point 9 (S9) corresponds to the suction surface separation bubble, as discussed later. The ensemble-averaged unsteady pressure results are decomposed into Fourier harmonic components:

$$p(t) = a_0 + \sum_n [a_n \cos(n\omega t) + b_n \sin(n\omega t)]$$
$$= a_0 + \sum_n Ap_n \sin(n\omega t + \phi_n) \qquad (n = 1, 2, 3, \ldots) \quad (2)$$

C. Tubing Correction by Transfer Function Method

When using an externally mounted transducer for blade surface unsteady pressure measurements, we have to address the issue of signal distortion caused by tubing connection. A simple direct procedure as used by Bell[7] is to directly measure the phase lag and amplitude attenuation for a certain tube length. A more general correction method is adopted in the present work, based on the transfer function method originally proposed by Irwin et al.[18] and applied to vehicle aerodynamics measurements by Sims-Williams.[19]

To utilize this approach, unsteady pressures are most conveniently expressed in a complex form. The tubing transfer function is obtained experimentally. The test pressure signals with a range of frequency concerned are recorded by a reference pressure transducer directly and by another pressure transducer via a tubing length used for actual unsteady pressure measurements. The complex tubing system transfer function $TF(f)$ is expressed as

$$TF(f) = B(f)/A(f) \quad (3)$$

where $A(f)$ is the complex Fourier coefficient of the pressure measured by the reference transducer and $B(f)$ is the complex Fourier coefficient of the distorted pressure.

Correction on the measured data for a given tube length and frequency is straightforward once the corresponding transfer function is known. The distorted signal is logged in the time domain and transformed into its Fourier coefficients in the frequency domain by fast Fourier transform (FFT), which is corrected using the already known transfer function:

$$A'(f) = B(f)/TF(f) \quad (4)$$

The corrected signal $A'(f)$ is then transformed back to the time domain using the inverse FFT. By using this technique, both the amplitude distortion and the phase shift of the unsteady signal are systematically corrected. This tubing correction method is more generally applicable than the previous treatments by He[4] and Bell.[7]

D. Repeatability of Unsteady Measurement

The use of externally mounted pressure transducers requires a series of tests to obtain the responses of all blades in the cascade. Hence, there is an additional need to ensure a good repeatability of measurements. Forty sets of unsteady pressure measurements are performed at a midrange reduced frequency (k: 0.3) to experimentally examine the repeatability. The five tapping points are chosen from the midspan of the reference blade. The unsteady pressure signals are obtained by the experimental procedure just described. Figure 4 shows the results in the form of deviations from the mean in the first harmonic pressure amplitude for the five tapping points. The range of all deviations in the amplitudes normalized by the mean value is within ± 0.05. The deviations in phase angle fall within the range of ± 3 deg. The corresponding standard deviation is 0.028 in $|Cp1|$ and 1.16 deg in phase angle. These deviations are negligibly small. Thus the results indicate a good repeatability.

E. Influence Coefficient Method

The influence coefficient method[10] provides an effective method to obtain the tuned cascade data by oscillating only one blade. The seven blades in the present cascade are numbered from -3 to $+3$, as shown in Fig. 2. The middle blade (blade 0) is oscillated. The induced unsteady pressures on the middle blade itself and its stationary

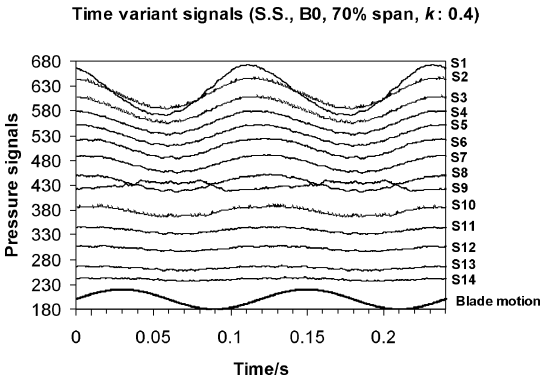

Fig. 3 Ensemble-averaged unsteady pressure (Pa) on suction surface of blade 0 (70% span, $k = 0.4$, 50 periods).

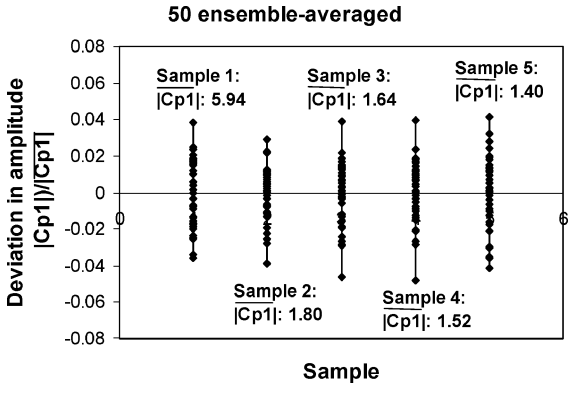

Fig. 4 Deviations in the first harmonic pressure amplitudes for five sample points (normalized by the corresponding averaged amplitudes).

neighbors are measured. Under a linear assumption these measured unsteady pressures can be superimposed to give the unsteady pressures for a tuned cascade at the same vibration frequency with a constant interblade phase angle. Effectively what we measure are the influence coefficients from the blade under consideration and its neighboring blades. For the equivalent tuned cascade the first harmonic unsteady pressure coefficient Cp_1 can be expressed as a sum of first harmonic influence coefficients $Cp_1(n)$ from all blades of the cascade (seven blades in this case):

$$Cp_1 = \sum_{n=-3}^{+3} Cp_1(n)e^{-in\sigma} \tag{5}$$

where σ is defined as positive when blade + 1 leads blade 0, corresponding to a forward traveling wave mode.

III. Experimental Results

Steady and unsteady results will be presented for a nominal aerodynamic loading (around 0-deg incidence). For steady flow conditions blade–blade periodicity needs to be clarified, and basic three-dimensional steady end-wall flow patterns need to be examined. The unsteady results and discussions are then presented to address several issues: the validity of the influence coefficient method (including the linearity), the unsteady three-dimensional behavior, and finally the effect of tip clearance.

A. Steady Flow

1. Inlet Flow Condition

The inlet flow condition is measured by a three-hole probe at the inlet measurement plane, located at half-chord length upstream of the cascade leading edge. The passage-averaged inlet total pressure loss distribution from blade midspan to tip is shown in Fig. 5. Apparently, higher total pressure losses near the end wall are caused by the inlet end-wall boundary layer, starting to grow about one chord upstream of the blade leading edge. Neglecting the tip-clearance effect on the upstream flow, the cascade can be assumed symmetrical to the midspan and so is the total pressure loss distribution. The definition of the local total pressure loss coefficient is

$$Y = \frac{P_{01} - P_0}{P_{01} - P_2} \tag{6}$$

Here, P_0 is the total pressure recorded at half-chord length upstream of the cascade, P_{01} is the inlet total pressure measured at a midspan position one chord length upstream of the cascade by using pitot-static tube, and P_2 is the ambient pressure to which the cascade exit is subjected.

2. Blade–Blade Periodicity

Prior to unsteady measurements, an effort is made to verify and improve the blade–blade periodicity. In particular, the blade–blade periodicity for the middle three blades is important for the unsteady flow experiment by using the influence coefficient method because the main unsteady responses, as we will see in the unsteady result section, come from the middle three blades. After a certain trial-and-error adjustment of the upstream side bleeding, a good blade–blade periodicity is achieved with the deviations of surface pressures on the middle three blades within a 5% range at all span locations. Figures 6 and 7 show the static pressure distributions at 50% span and 90% span, respectively. The main differences show up on the suction surface near the leading edge as well as in the near end-wall region, as expected. Overall, this reasonably good blade–blade periodicity forms a sound basis for unsteady flow measurements.

3. Main Steady Flow Characteristics

To demonstrate the spanwise steady loading of the cascade at the nominal flow condition, static surface pressure distributions at six span sections on blade 0 are presented in Fig. 8. It is noticeable that there is an abrupt pressure variation at 55% chord between the

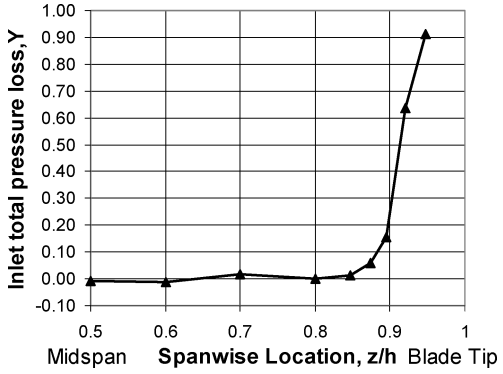

Fig. 5 Inlet total pressure loss at a nominal aerodynamic loading without blade tip gap.

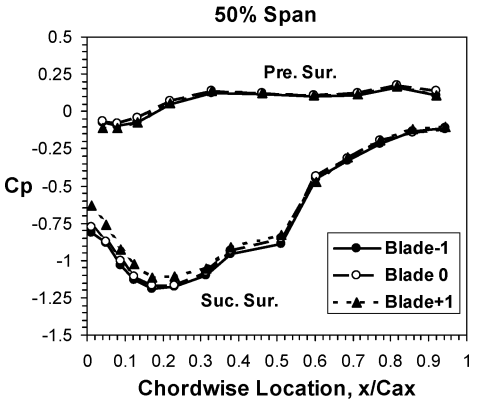

Fig. 6 Steady pressure distributions at 50% span.

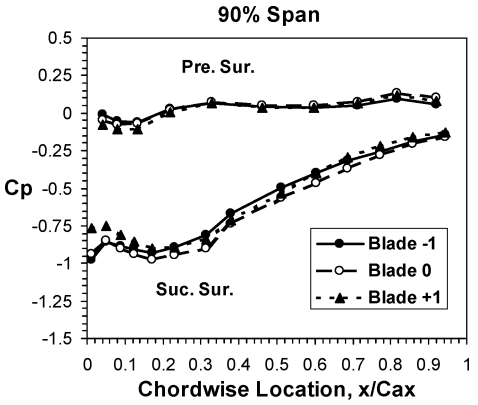

Fig. 7 Steady pressure distribution at 90% span.

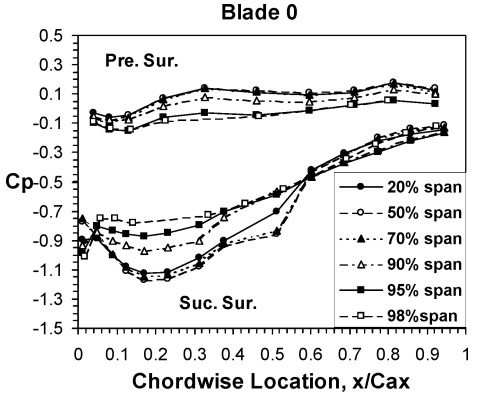

Fig. 8 Steady pressure distributions at different spanwise sections on blade 0.

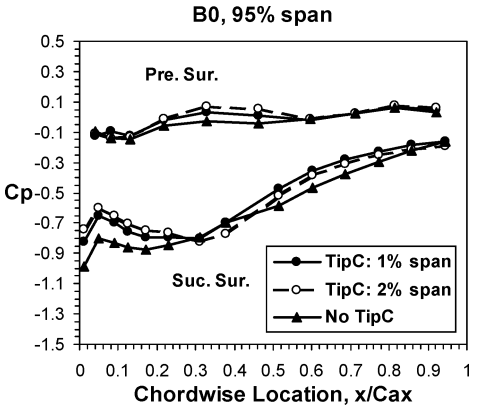

Fig. 9 Steady pressure distributions with three settings of tip clearance at 95% span.

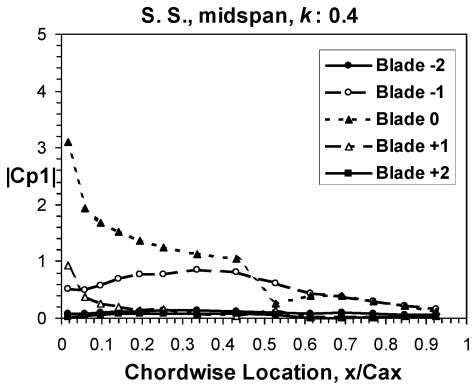

Fig. 10 Unsteady pressure amplitudes caused by oscillation of blade 0 (midspan at $k = 0.4$).

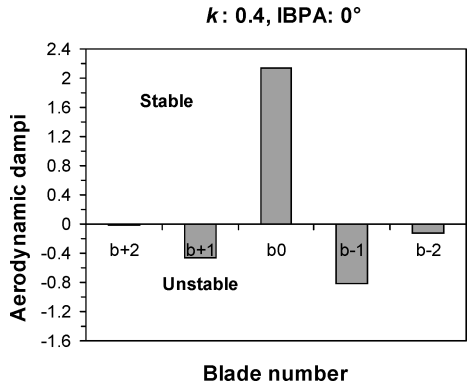

Fig. 11 Aerodamping components contributed from middle five blades (IBPA 0 deg and $k = 0.4$).

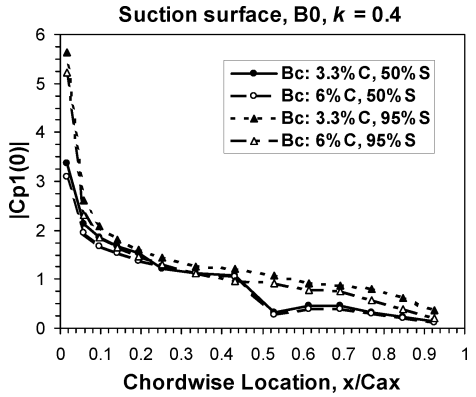

Fig. 12 Amplitudes of the first harmonic pressure coefficients (at 50 and 95% spans) at two bending oscillation amplitudes (3.3 and 6% C).

midspan and 70% span on the suction surface. This is identified as a bubble-type laminar flow separation and is consistent with the unsteady pressure results (as indicated by the pressure time trace S9 in Fig. 3). Although there are no tappings located at 30% span, the two-dimensional separation bubble is clearly identifiable at 70% span and hence can be assumed to exist at least between 30 and 70% span because the steady flowfield is largely symmetrical to the midspan. The Reynolds number in the present case is relatively low ($Re = 1.95 \times 10^5$). At higher and more realistic Reynolds numbers in compressors, there is the same type of laminar separation bubble, though the chordwise location is more upstream[16] for the same blade geometry.

The flow unloading in the end-wall region (from 90% span) is apparent (Fig. 8), which results from the blade passage vortex as reported in Sasaki's work.[17] Another unloading effect is identified because of the tip clearance. Blade-surface steady pressure distributions at the three settings of tip clearance at 95% span (near blade tip) are presented in Fig. 9 to provide the aerodynamic background for the unsteady pressure measurements. The blade loading is evidently changed as the tip clearance is increased. Measurable variations in blade loading are observed with the maximum tip clearance (2% span). The unloading can be observed between the leading edge and 34% chord at 95% span location on the suction surface. Then a small reloading takes place at 40% chord with the 2% span tip clearance. A similar trend is reported by Kang and Hirsch.[12] They give an explanation of the reloading resulting from the low-pressure core of the tip leakage vortex. Compared with that on the suction surface, the loading on the pressure surface is only slightly affected by the tip clearance. Overall, significant changes in blade loading caused by increasing tip clearance are located in the blade near tip region (90% span outwards).

B. Unsteady Flow

1. Validity of Influence Coefficient Method

For validity of the influence coefficient method, two aspects are essentially required. One is a sufficient convergence (decay) of unsteady pressure responses on those blades far from the reference blade to ensure that only a small number of blades need to be measured. Another is the linearity of unsteady aerodynamics responses.

The convergence of the influence coefficients is demonstrated in Fig. 10, which shows the first harmonic pressure coefficients on the suction surfaces of blade −2 to blade +2 when blade 0 is oscillated. The unsteady aerodynamic responses on the suction surfaces converge quite quickly with increasing distance from the reference (oscillating) blade. The results on the pressure surfaces (not shown) converge even faster. The overall aerodynamic damping components contributed from the middle five blades to a tuned cascade at 0-deg IBPA also confirm the same trend (Fig. 11).

The linear assumption is not only fundamental for the validity of the influence coefficient method, but also of general interest to unsteady aerodynamic modeling. For the present test rig there is a separation bubble on the suction surface and a large area of three-dimensional vortical flow near the end wall. Therefore, the linearity issue needs to be experimentally checked. This is conducted by comparing unsteady aerodynamic responses obtained at two blade vibration (bending) amplitudes. Figure 12 shows the amplitudes of the first harmonic pressure coefficient at 50 and 95% spans of the reference blade and Fig. 13 for the phase angles. The pressure amplitudes (normalized by the corresponding blade vibration amplitude, respectively) are almost identical for both cases. The phase angles also show good agreement for the whole pressure surface and the majority of the suction surface apart from the region subject to the separation bubble around 50% chord with a localized effect, as indicated by He.[4] Regarding the second harmonic pressures (Fig. 14), a large peak in the second harmonic amplitude is seen in the suction surface separation bubble region, as expected. A smaller peak is observed around 30% chord on the pressure surface at the midspan section, where there is a change of the steady flow gradient

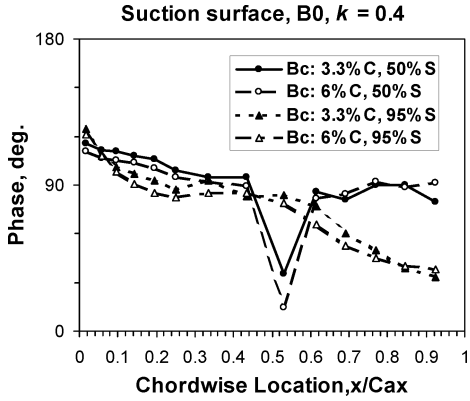

Fig. 13 Phase angles of the first harmonic pressure coefficients (at 50 and 95% spans) at two bending oscillation amplitudes (3.3 and 6%C).

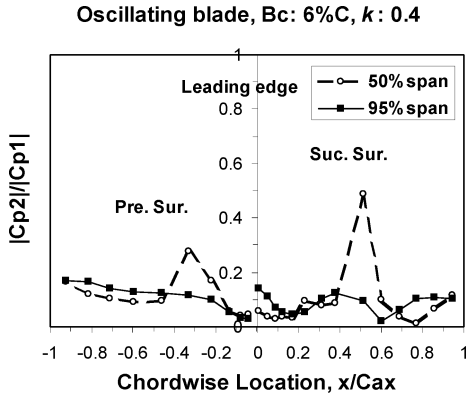

Fig. 14 Relative amplitudes of the second harmonic pressure coefficient at 50 and 90% spans.

(as indicated in Fig. 8) and the first harmonic pressure is also relatively low. Overall, the unsteady flow behavior is shown to be predominantly linear.

2. Main Unsteady Flow Characteristics

The amplitude and phase of the first harmonic pressure for 90-deg IBPA and 180-deg IBPA at $k = 0.4$ are presented in Figs. 15 and 16 to demonstrate the main unsteady flow characteristics and the effect of interblade phase angle on cascade aeroelastic stability. The existence of the flow separation bubble on the suction surface can be identified from Figs. 15 and 16, which is consistent with the steady pressure distributions shown in Fig. 8. There are abrupt changes in phase and amplitude at 54% chord between 50 and 70% spans on the suction surface for two IBPAs, which is a typical feature of the separation bubble as documented by He[4] and Buffum et al.[5] The largely two-dimensional separation bubble disappears in the end-wall regions as a result of the strong influence of the local three-dimensional secondary flow vortex structure.

The largely constant amplitudes of unsteady pressures at different spanwise locations illustrate a strong three-dimensional behavior of unsteady aerodynamics. As shown in Fig. 15, the largest spanwise variation in the amplitude occurs in the leading-edge region for 90-deg IBPA. But even in this case, the amplitude at 95% span is just two and one-half times greater than that obtained at 20% span, whereas the local blade vibration amplitudes differ by five times. This nonproportional distribution of the unsteady amplitude at different span locations indicates that the unsteady pressure wave has instantaneous radial interaction. This fully three-dimensional feature certainly challenges the validity of the traditional quasi-three-dimensional strip theory. A similar feature has been identified computationally by Hall and Lorence[20] for oscillating cascades using a three-dimensional linearized Euler solver and experimentally by Bell and He[8] for a single oscillating turbine blade.

The pronounced effect of the IBPA on the amplitude and phase can also be seen in Figs. 15 and 16. The trend of the amplitudes on both surfaces is the same for two IBPAs, but the slopes are steeper

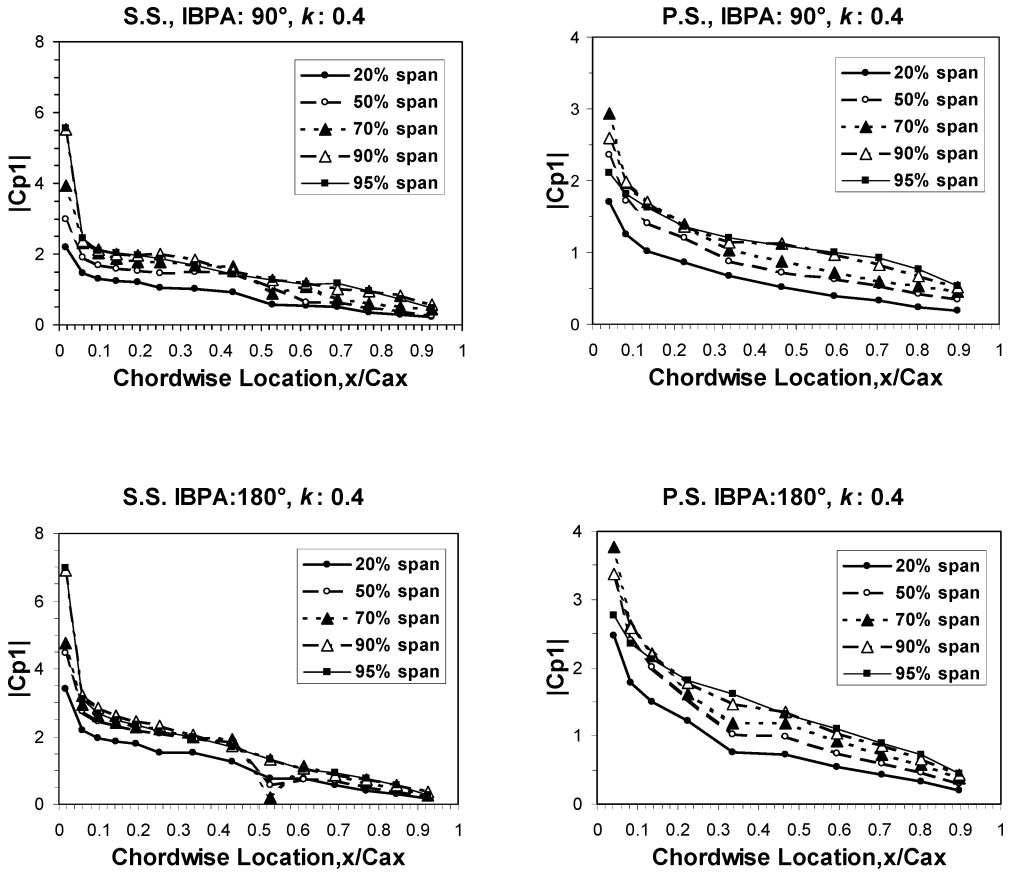

Fig. 15 The first harmonic pressure amplitude distributions at IBPA = 90 deg (top) and IBPA = 180 deg (bottom).

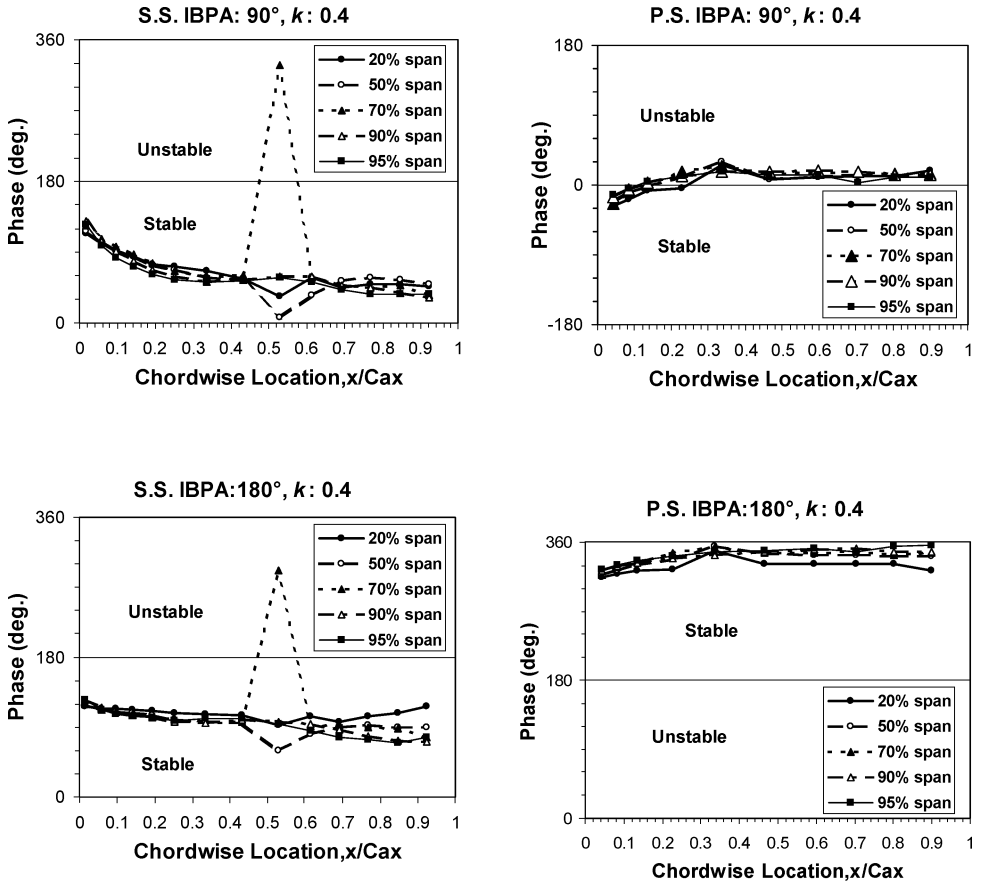

Fig. 16 The first harmonic pressure phase angle distributions at IBPA = 90 deg (top) and IBPA = 180 deg (bottom).

for 180-deg IBPA (Fig. 15), that is, the unsteady pressure amplitude increases largely over the frontal half of the chord on both surfaces. From Fig. 16 it is seen that the interblade phase angle has a significant influence on the cascade stability by changing the pressure phase angle. The phase leading the blade motion over the suction surface and lagging the motion over the pressure surface indicates an aeroelastically stable condition. At 90-deg IBPA the phase shows a stable condition on the suction surface except for the position at 55% chord at 70% span caused by the presence of the separation bubble. This is also the case for 180-deg IBPA. On the pressure surface, however, the phase indicates a destabilizing contribution after 15% chord at 90-deg IBPA. In contrast to this, at 180-deg IBPA the phase distribution indicates a stabilizing contribution to the aerodynamic damping over the entire pressure surface.

3. *Aerodynamic Damping for Tuned Cascade*

The unsteady pressures over blade surfaces are integrated to produce the overall aerodynamic damping, which is a direct measure of the energy transferred from the flowfield to the oscillating blade and hence indicates the cascade aeroelastic stability. To compare the variation in the unsteady pressure response with IBPA and reduced frequency, Fig. 17 plots the overall aerodynamic damping as a function of the interblade phase angle at three reduced frequencies. The pressures around the leading and the trailing edges are taken from the nearest tappings. The cascade is indicated as being aeroelastically stable by the positive values of the overall aerodynamic damping over the entire range of interblade phase angles at three reduced frequencies. The aerodamping curves on the damping–IBPA diagram seem to follow a trend that as the frequency decreases the sinusoidal damping curve moves downward as well as rightward. The least stable IBPA is 30 deg at $k = 0.4$ and 40 deg at $k = 0.2$, corresponding to a forward-traveling wave mode with one or two nodal diameters (depending on the total number of blades in a real blade row). The trend suggests that at a lower frequency the least

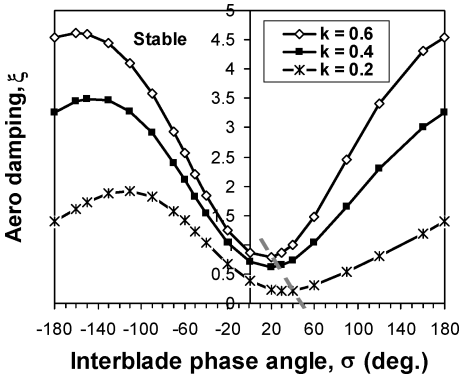

Fig. 17 Overall aerodynamic damping at three reduced frequencies: – – –, trend of the least stable points with different frequencies.

stable forward-traveling wave mode should have a larger number of nodal diameters. On the other hand, the number of nodal diameters at the minimum damping point will decrease at a higher frequency. Following this trend, it might be possible that for a given high frequency the minimum aerodamping, which might well be positive, even occurs at a negative interblade phase angle, corresponding to a backward-traveling wave mode.

4. *Tip-Clearance Effect*

The tip-clearance effect is examined by comparing unsteady responses at two settings of tip clearance (1% span and 2% span) to that with no tip clearance. At the setting of zero tip clearance, the gap between the oscillating blade and the end wall is covered by a piece of dense sponge, and there is effectively no gap between the stationary blades and the side wall. It is recognized that the relative motion of end wall caused by rotation in a real rotor row is not included in the present work.

Figure 18 shows the aerodynamic damping against interblade phase angles for each tip-gap setting. The extreme damping conditions affected by the different tip leakage flows would also change slightly the corresponding interblade phase angles. It can be seen that the maximum destabilizing influence of the tip gap is at 30-deg IBPA with a tip clearance of 2% span, at which the minimum damping has been reduced by around 27% compared to that at the nominal zero tip-gap condition at the same frequency. This tip-gap destabilizing effect can be compared with how much the minimum aerodamping is reduced when the reduced frequency is halved from 0.4 to 0.2 (Fig. 17).

To inspect in detail the influence of tip gap on the unsteady pressure responses, the amplitudes and phase angles of the first harmonic pressure at 95% span at 30-deg IBPA are presented in Figs. 19 and 20 with the three settings of the tip gap. The amplitudes consistently decrease in the leading-edge region on the suction surface, and the influenced region extends with increase of the tip gap. The frontal region with decreased pressure amplitude (up to 25%C) is followed by a region with increased amplitude (20–45%C) compared to that with no tip gap. The region of increased amplitude corresponds to the development of the tip leakage flow, although the reloading only can be identified at 40% chord with 2% span tip clearance (Fig. 9). A smaller change in amplitude is observed on the first part of the pressure surface (Fig. 19). Regarding the phase angles (Fig. 20), two points should also be noted. Firstly the phase angle in the region 40–70% chord on the suction surface decreases noticeably, and hence the local aerodamping becomes less stable as the tip gap increases. Secondly the phase in the rear part on the pressure surface (40–100%C) increases, and thus the area becomes more destabilized with the increase in the tip gap. Generally the decreased amplitude of the first harmonic pressure with increasing tip gap corresponds to the frontal unloading area in the steady flow results shown in Fig. 9, similar to that reported by Bell[7] for an isolated oscillating turbine blade. The variations in the aerodynamic damping for three settings of tip gap at 30-deg IBPA (Fig. 18) mainly result from the changes in the unsteady pressure amplitudes on the suction surface and the first part of the pressure surface. It is also observed that the tip-clearance destabilizing effect on the cascade stability is qualitatively independent of interblade phase angles.

Figure 21 presents the spanwise distributions of the local aerodynamic damping at the largest tip gap compared to that at the nominal zero tip gap for the two IBPAs corresponding to the damping extrema. Note that the influence of tip gap is not localized in the tip region because of the unsteady three-dimensional effect (radial instantaneous interaction), although it is more pronounced near the tip. At the least stable IBPA 30 deg, the local aerodynamic damping in the region of 90 ~ 95% span is decreased by around 45% when the tip gap is increased to that of 2% span.

Finally, in the present rigid-body configuration the oscillation amplitude varies linearly along span, whereas practical flexible blades in first flap/bending mode will have relatively larger deflection near the tip (and hence larger local modal damping work). Hence, we might expect a larger influence of the tip-clearance gap on the overall

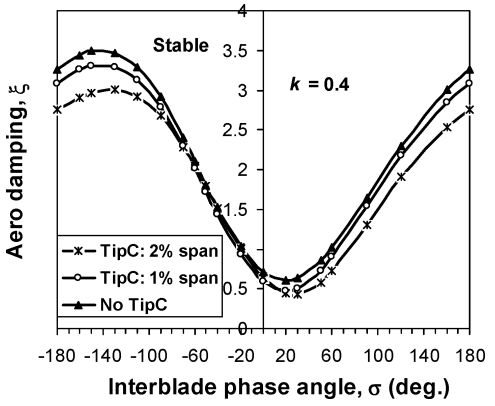

Fig. 18 Overall aerodynamic damping for three tip-gap settings: $k = 0.4$.

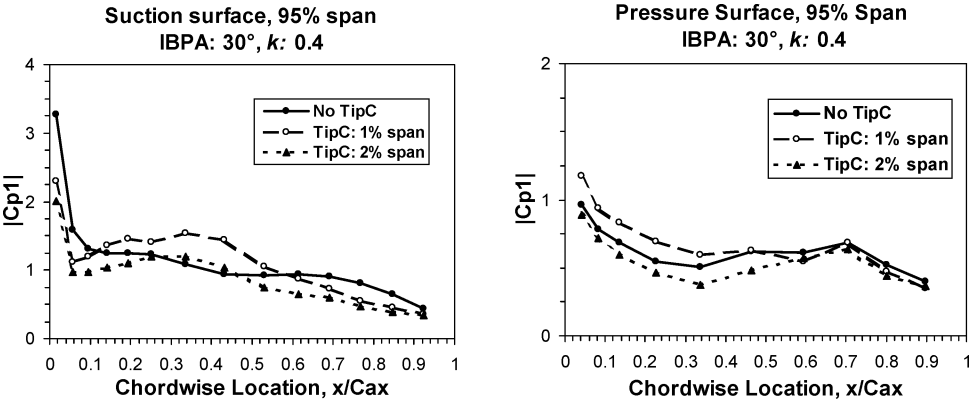

Fig. 19 Amplitudes of unsteady pressure at 95% span for three tip-gap settings: IBPA = 30 deg and $k = 0.4$.

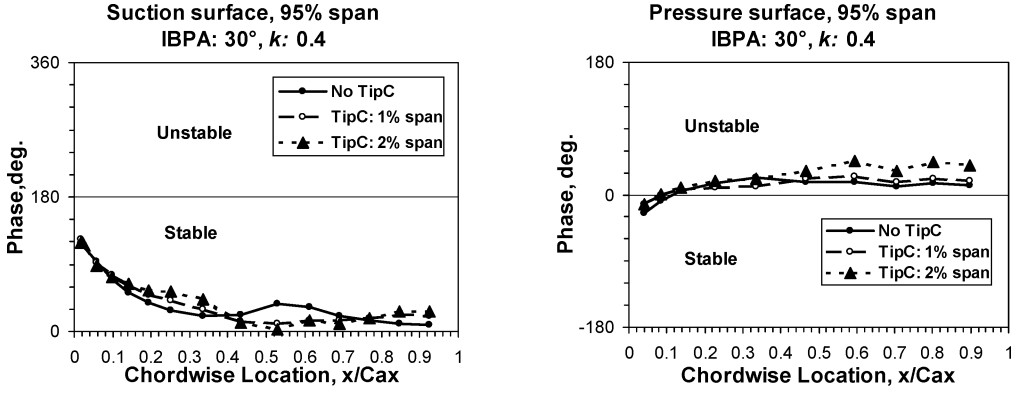

Fig. 20 Phase angles of unsteady pressure at 95% span for three tip-gap settings: IBPA = 30 deg and $k = 0.4$.

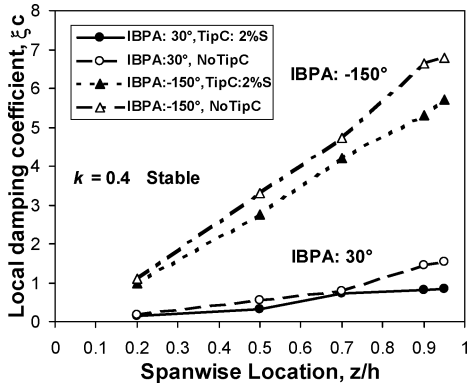

Fig. 21 Spanwise local aerodamping coefficients with and without tip clearance: IBPA = 30 deg and −150 deg at $k = 0.4$.

aerodynamic damping for real flexible blades than that observed in the present experiment. In relation to computational modeling, the tip-clearance destabilizing effect would imply that a computational method without tip-clearance modeling might lead to an overstable prediction of flutter onset condition.

IV. Conclusions

An experiment on unsteady flow of a linear three-dimensional oscillating compressor cascade is carried out. To the authors' knowledge, this is the first-of-its-kind three-dimensional unsteady pressure data in oscillating cascades, which can be directly used for validation of three-dimensional computational methods for turbomachinery aeromechanics applications.

The unsteady pressure data for an oscillating cascade are obtained by use of off-board transducers with tubing transfer function correction and the influence coefficient method. The unsteady aerodynamic response is shown to be largely linear. The aerodynamic damping indicates a trend that as the reduced frequency decreases the interblade phase angle of the least stable condition increases. The results also provide clear experimental evidence on the three-dimensional unsteady behavior caused by the spanwise instantaneous interaction. Hence, a quasi-three-dimensional approach will be deemed to be erroneous.

The tip-clearance gap is shown to have a destabilizing effect for all interblade phase angles. Detailed unsteady pressure results show that the region with reduced aerodynamic damping coincides with that of unloading in steady flow. The tip-clearance destabilizing effect is shown to influence most of blade span. The total aerodynamic damping at the least stable interblade phase angle is reduced by 27%, when the tip gap is increased from nearly zero to 2% span.

Acknowledgments

The financial sponsorship from ALSTOM, UK, Ltd., is gratefully acknowledged. The authors would like to thank R. Wells, Y. S. Li, and W. Ning (ALSTOM Industrial Gas Turbines) and D. Bell (ALSTOM Steam Turbines) for their support. They would also like to thank D. B. Sims-Williams of the School of Engineering for the help regarding application of the transfer function method.

References

[1]Carta, F. O., and St. Hilaire, A. O., "Experimentally Determined Stability Parameters of a Subsonic Cascade Oscillating Near Stall," *Journal of Engineering for Power*, Vol. 100, No. 1, 1978, pp. 111–120.

[2]Carta, F. O., and St. Hilaire, A. O., "Effect of Interblade Phase Angle and Incidence Angle on Cascade Pitching Stability," *Journal of Engineering for Power*, Vol. 102, No. 2, 1980, pp. 391–396.

[3]Bölcs, A., and Fransson, T. H., "Aeroelasticity in Turbomachines Comparison of Theoretical and Experimental Cascade Results," Communication du Lab. de Thermique Appliquée et de Turbomachines, EPFL, No. 13, Lausanne, Switzerland, June 1986.

[4]He, L., "Unsteady Flow in Oscillating Turbine Cascades: Part 1—Linear Cascade Experiment," *Journal of Turbomachinery*, Vol. 120, No. 2, 1998, pp. 262–268.

[5]Buffum, D. H., Capece, V. R., King, A. J., and El-Aini, Y. M., "Oscillating Cascade Aerodynamics at Large Mean Incidence," *Journal of Turbomachinery*, Vol. 120, No. 1, 1998, pp. 122–130.

[6]Lepicovsky, J., McFarland, E. R., Capece, V. R., and Hayden, J., "Unsteady Pressures in a Transonic Fan Cascade Due to a Single Oscillating Airfoil," American Society of Mechanical Engineers, Paper GT-2002-30312, June 2002.

[7]Bell, D. L., "Three Dimensional Unsteady Flow for an Oscillating Turbine Blade," Ph.D. Dissertation, School of Engineering, Univ. of Durham, England, U.K., 1999.

[8]Bell, D. L., and He, L., "Three-Dimensional Unsteady Flow for an Oscillating Turbine Blade and the Influence of Tip leakage," *Journal of Turbomachinery*, Vol. 122, No. 1, 2000, pp. 93–101.

[9]Queune, O. J. R., and He, L., "Experimental Study of 3D Unsteady Flow Around Oscillating Blade with Part-Span Separation," *Journal of Turbomachinery*, Vol. 123, No. 3, 2001, pp. 519–525.

[10]Hanamura, Y., Tanaka, H., and Yamaguchi, K., "A Simplified Method to Measure Unsteady Forces Acting on the Vibrating Blades in Cascade," *Bulletin of the JSME*, Vol. 23, No. 180, June 1980, pp. 880–887.

[11]Hoying, D. A., Tan, C. S., Vo, H. D., and Greitzer, E. M., "Role of Blade Passage Flow Structures in Axial Compressor Rotating Stall Inception," *Journal of Turbomachinery*, Vol. 121, No. 4, 1999, pp. 735–742.

[12]Kang, S., and Hirsch, C., "Experimental Study on the Three-Dimensional Flow Within a Compressor Cascade with Tip Clearance: Part 1—Velocity and Pressure Fields," *Journal of Turbomachinery*, Vol. 115, No. 3, 1993, pp. 435–443.

[13]Pandya, A., and Lakshminarayana, B., "Investigation of the Tip Clearance Flow Inside and at the Exit of a Compressor Rotor Passage—Part 1: Mean Velocity Field," *Journal of Engineering for Power*, Vol. 105, No. 1, 1983, pp. 1–12.

[14]Watanabe, T., and Kaji, S., "Experimental Study on Unsteady Aerodynamic Characteristics of an Oscillating Cascade with Tip Clearance," *Bulletin of the JSME*, Vol. 31, No. 4, 1988, pp. 660–667.

[15]Elazar, Y., and Shreeve, R. P., "Viscous Flow in a Controlled Diffusion Compressor Cascade with Increasing Incidence," *Journal of Turbomachinery*, Vol. 112, No. 2, 1990, pp. 256–266.

[16]Sanger, N. L., and Shreeve, R. P., "Comparison of Calculated and Experimental Cascade Performance for Controlled-Diffusion Compressor Stator Blading," *Journal of Turbomachinery*, Vol. 108, No. 1, 1986, pp. 42–50.

[17]Sasaki, T., and Breugelmans, F., "Comparison of Sweep and Dihedral Effects on Compressor Cascade Performance," *Journal of Turbomachinery*, Vol. 120, No. 3, 1998, pp. 454–464.

[18]Irwin, H. P. A. H., Cooper, K. R., and Girard, R., "Correction of Distortion Effects Caused by Tubing Systems in Measurements of Fluctuating Pressures," *Journal of Industrial Aerodynamics*, Vol. 5, Nos. 1–2, 1979, pp. 93–107.

[19]Sims-Williams, D., "Self-Excited Aerodynamic Unsteadiness Associated with Passenger Cars," Ph.D. Dissertation, School of Engineering, Univ. of Durham, England, U.K., 2001.

[20]Hall, K. C., and Lorence, C. B., "Calculation of Three-Dimensional Unsteady Flows in Turbomachinery Using the Linearized Harmonic Euler Equations," *Journal of Turbomachinery*, Vol. 115, No. 4, 1993, pp. 800–809.